# Обзор ArXiv: astro-ph, 16-28 марта 2018 года

От Сильченко О.К.

# Astro-ph: 1803.07745

## Formation of S0s via disc accretion around high-redshift compact ellipticals

J.D. Diaz[1⋆], Kenji Bekki,[1] Duncan A. Forbes,[2] Warrick J. Couch,[2,3]
Michael J. Drinkwater[4] and Simon Deeley[4]
[1] *ICRAR, M468, The University of Western Australia 35 Stirling Highway, Crawley Western Australia, 6009, Australia*
[2] *Centre for Astrophysics & Supercomputing, Swinburne University, Hawthorn, VIC 3122, Australia*
[3] *Australian Astronomical Observatory, 105 Delhi Rd, North Ryde, NSW 2113, Australia*
[4] *School of Mathematics and Physics, University of Queensland, QLD 4072, Australia*

**ABSTRACT**

We present hydrodynamical N-body models which demonstrate that elliptical galaxies can transform into S0s by acquiring a disc. In particular, we show that the merger with a massive gas-rich satellite can lead to the formation of a baryonic disc around an elliptical. We model the elliptical as a massive, compact galaxy which could be observed as a 'red nugget' in the high-$z$ universe. This scenario contrasts with existing S0 formation scenarios in the literature in two important ways. First, the progenitor is an elliptical galaxy whereas

# Любимая модель

**Table 1.** Description of the basic parameter values for the simulated compact elliptical and satellite spiral galaxy in the fiducial model.

| | Elliptical | Satellite |
|---|---|---|
| DM halo mass ($\times 10^{12} M_\odot$) | 1.0 | 0.3 |
| Virial radius (kpc) | 81.7 | 134.2 |
| $c^\dagger$ | 5 | 12 |
| Spheroid mass ($\times 10^{10} M_\odot$) | 6.0 | – |
| Spheroid half mass radius (kpc) | 0.85 | – |
| Stellar disc mass ($\times 10^{10} M_\odot$) | - | 0.18 |
| Gas disc mass ($\times 10^{10} M_\odot$) | - | 1.26 |
| Stellar disc size (kpc) | - | 9.6 |
| Gas disc size (kpc) | - | 9.6 |
| Initial gas metallicity ([Fe/H] dex) | - | −0.52 |
| Gravitational softening length (pc) | 43 | 138 |
| Mass resolution ($\times 10^4 M_\odot$) | 30.0 | 1.8 |

$^\dagger$ $c$ is the concentration parameter in the NFW dark matter profile.

Спутник падает в орбитальной плоскости

# Упал!

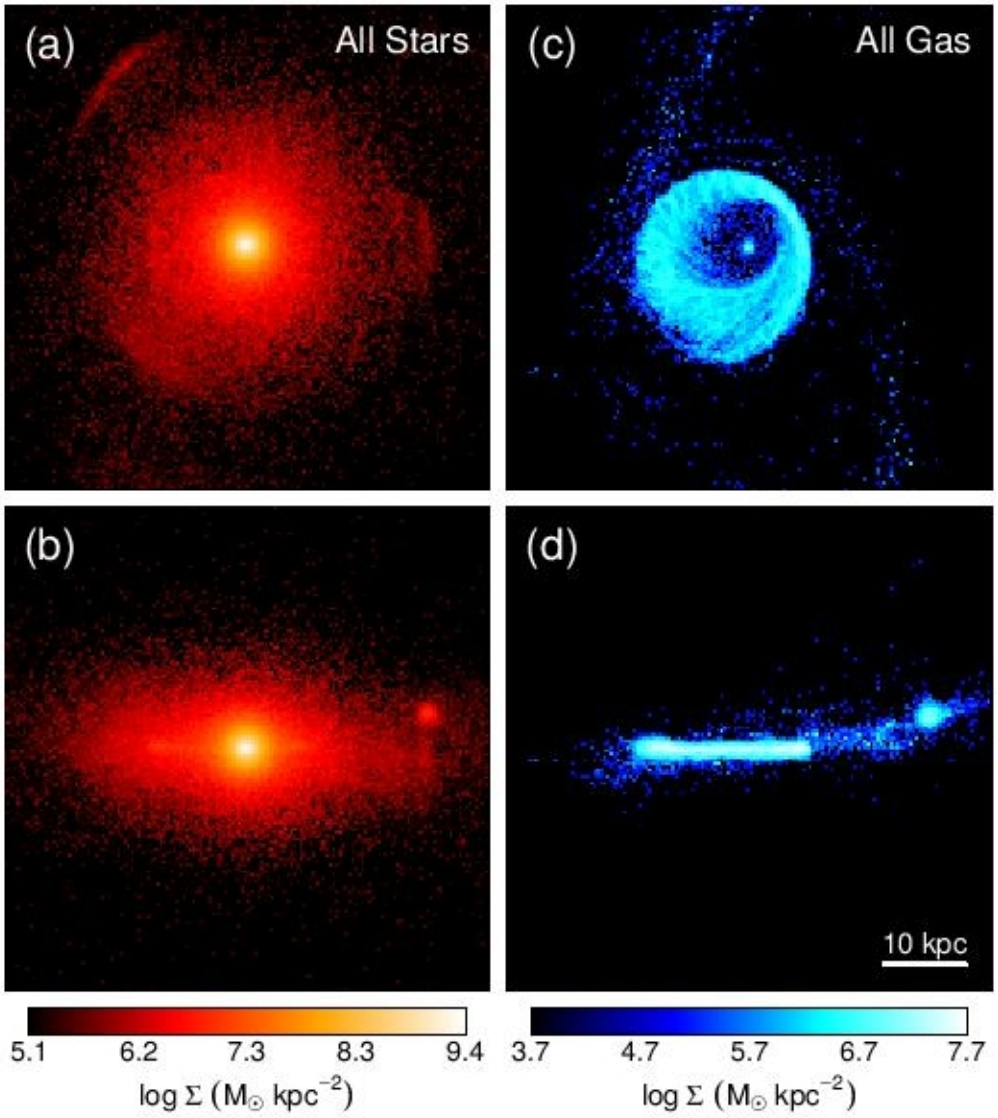


Face-on

Edge-on

# То же самое, разделенное на компоненты разного происхождения

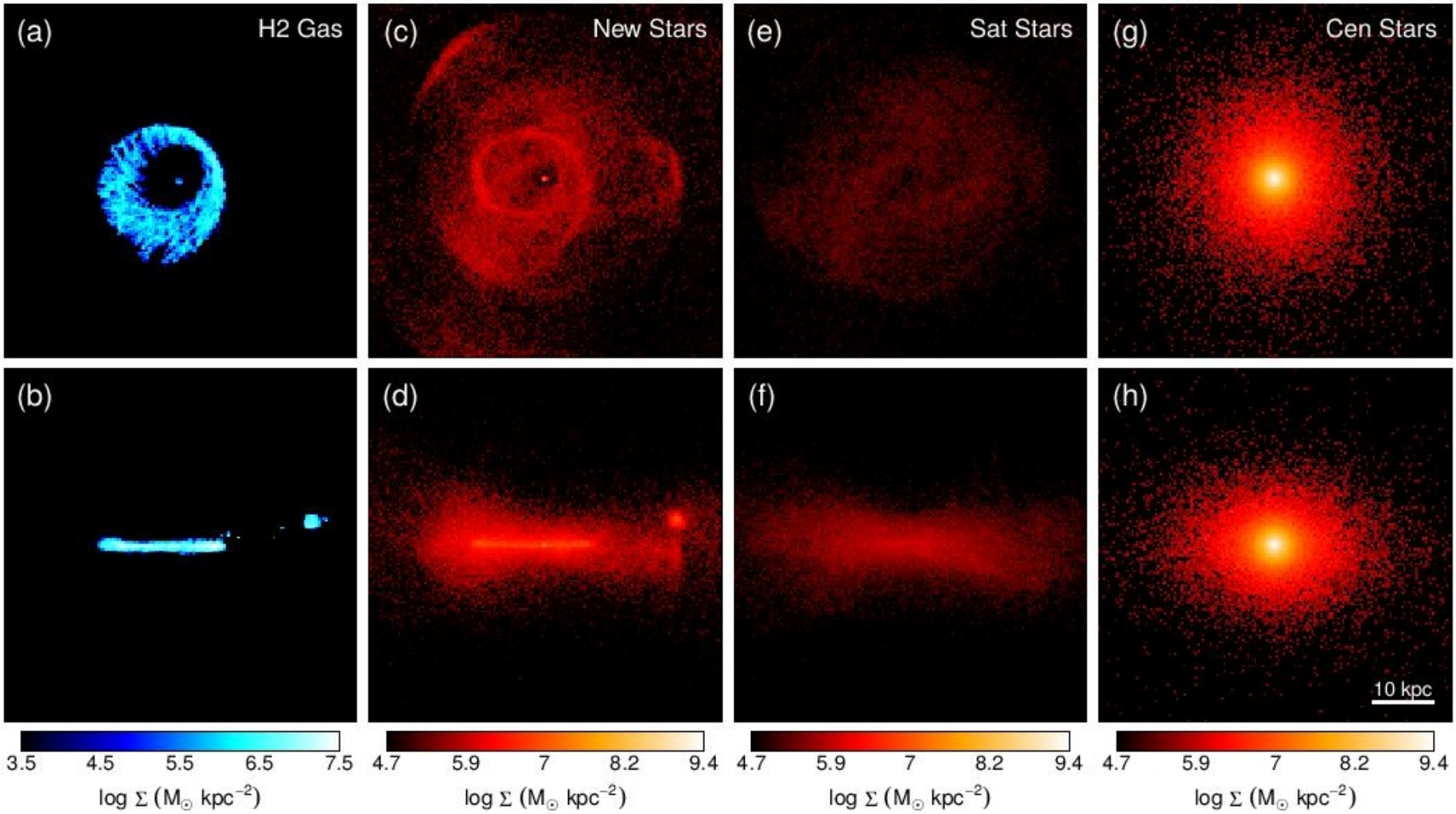

# Кинематика

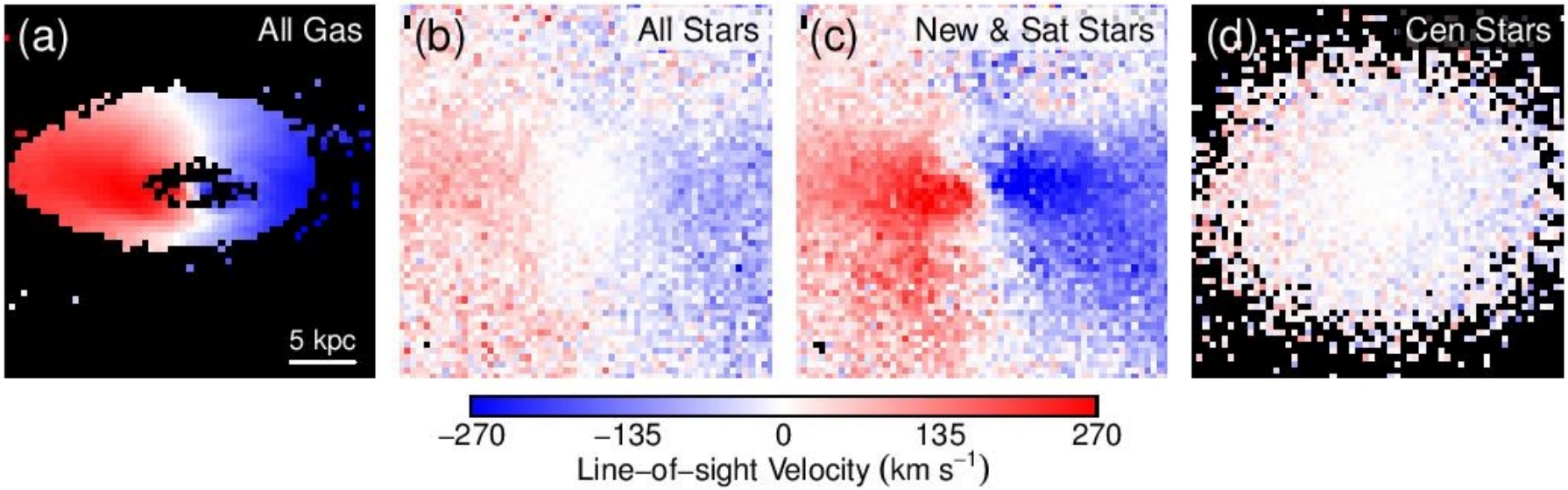


**Figure 5.** Two-dimensional velocity field of the fiducial model at the final time step with disc inclination set to 60° with respect to the plane of the sky. The line-of-sight velocity fields are separated by particle type: (a) all gas, (b) all stars, (c) stars formed out of gas plus stars initialized to the satellite, and (d) stars from the central elliptical galaxy. Note that panel (b) is the mass-weighted superposition of the stars in panels (c) and (d).

# Получился молодой экспоненциальный звездный диск

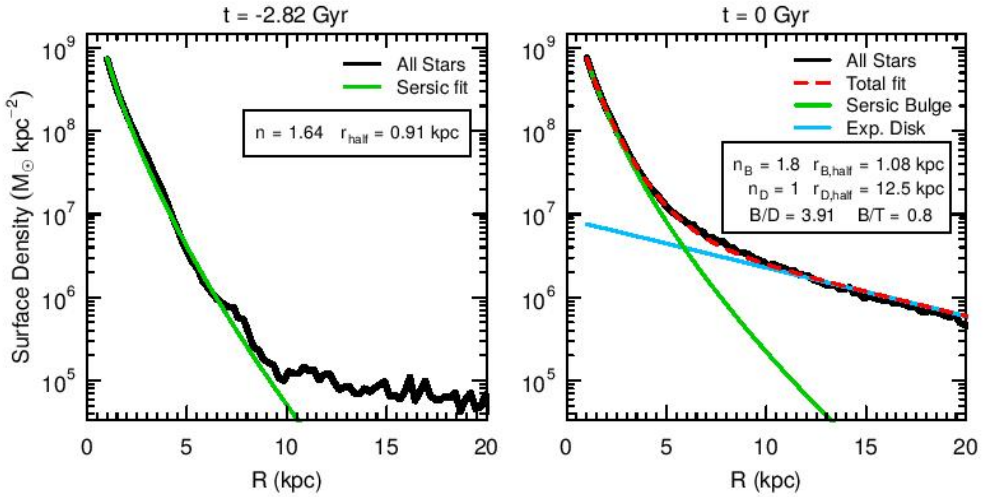


**Figure 3.** (*Left panel*) One-dimensional stellar surface density of the fiducial model at the start of the simulation ($t = -2.82$ Gyr) (black from the center of the elliptical galaxy. The fit is given by a single Sersic component with free index $n$ (green line), and the boxed inset parameter values of the fit. (*Right panel*) One-dimensional stellar surface density at the end of the simulation ($t = 0$ Gyr) along the cylinc disc (black line). The overall fit (red dashed line) is given by the sum of a bulge (Sersic component with free index $n_{\rm B}$; green line) and expor component with index $n_{\rm D} = 1$). The boxed inset gives the important parameter values of the fit along with the derived mass ratios between components. See text for details of the fit.

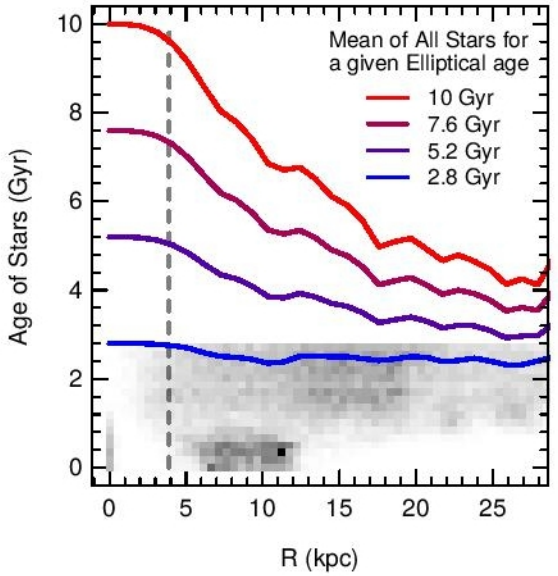


**Figure 7.** The age of stars as a function of radius in the fiducial model at $t = 0$ Gyr. The greyscale plot is a mass-weighted histogram of age versus radius for stars which formed during the simulation, where the greyscale varies from $5 \times 10^4$ $M_\odot$ per bin (white) to $10^7$ $M_\odot$ (black). These 'new stars' have an age which ranges from 0 Gyr (i.e. formed at the end of the simulation) to 2.82 Gyr (i.e. formed at the first time step) as determined by their epoch of formation. The coloured lines indicate the mass-weighted mean age of all stars in the model as a function of radius. The lines differ by the assumed age of the stars in the central Elliptical: 2.82 Gyr (blue),

# Astro-ph: 1803.08515

## SDSS-IV MaNGA: The Spatially Resolved Stellar Initial Mass Function in ~400 Early-Type Galaxies

Taniya Parikh[1⋆], Daniel Thomas[1], Claudia Maraston[1], Kyle B. Westfall[2], Daniel Goddard[1], Jianhui Lian[1], Sofia Meneses-Goytia[1], Amy Jones[3], Sam Vaughan[4] Brett H. Andrews[5], Matthew Bershady[6], Dmitry Bizyaev[7], Jonathan Brinkmann[7], Joel R. Brownstein[8], Kevin Bundy[2], Niv Drory[9], Eric Emsellem[10], David R. Law[11], Jeffrey A. Newman[12], Alexandre Roman-Lopes[13], David Wake[14], Renbin Yan[15], Zheng Zheng[16]

[1] *Institute of Cosmology and Gravitation, University of Portsmouth, 1-8 Burnaby Road, Portsmouth PO1 3FX, UK*
[2] *UCO/Lick Observatory, University of California, Santa Cruz, 1156 High St. Santa Cruz, CA 95064, USA*
[3] *Max-Planck-Institut für Astrophysik, Karl-Schwarzschild-Str. 1, D-85748 Garching, Germany*
[4] *Sub-department of Astrophysics, Department of Physics, University of Oxford, Denys Wilkinson Building, Keble Road, Oxford OX1 3RH*
[5] *PITT PACC, Department of Physics and Astronomy, University of Pittsburgh, Pittsburgh, PA 15260, USA*
[6] *Department of Astronomy, University of Wisconsin-Madison, 475N. Charter St., Madison WI 53703, USA*
[7] *Apache Point Observatory, P.O. Box 59, Sunspot, NM 88349*
[8] *Department of Physics and Astronomy, University of Utah, 115 S. 1400 E., Salt Lake City, UT 84112, USA*
[9] *McDonald Observatory, The University of Texas at Austin, 1 University Station, Austin, TX 78712, USA*
[10] *European Southern Observatory, Karl-Schwarzschild-Str. 2, 85748 Garching, Germany*
[11] *Space Telescope Science Institute, 3700 San Martin Drive, Baltimore, MD 21218, USA*
[12] *PITT PACC, Department of Physics and Astronomy, University of Pittsburgh, Pittsburgh, PA 15260, USA*
[13] *Departamento de Física, Facultad de Ciencias, Universidad de La Serena, Cisternas 1200, La Serena, Chile*
[14] *Department of Physics, University of North Carolina Asheville, One University Heights, Asheville, NC 28804, USA*
[15] *Department of Physics and Astronomy, University of Kentucky, 505 Rose Street, Lexington, KY 40506, USA*
[16] *National Astronomical Observatories of China, Chinese Academy of Sciences, 20A Datun Road, Beijing 100012, China*

# Сложили по 122 early-type галактики в трех диапазонах масс

The Color-enhanced sample supplements colour space that is otherwise under-represented relative to the overall galaxy population. The spatial resolution is $1-2$ kpc at the median redshift of the survey ($z \sim 0.03$), and the $r$-band S/N is $4-8$ Å$^{-1}$, for each $2''$ fibre, at the outskirts of MaNGA galaxies. For more detail on the survey we refer the reader to Law et al. (2015) for MaNGA's observing strategy, to Yan et al. (2016a) for the spectrophotometry calibration, to Wake et al. (2017) for the survey design, and to Yan et al. (2016b) for the initial performance.

*2.1.1 Galaxy sample*

We make use of data taken during the first two years of survey operations, equivalent to SDSS's fourteenth data release (Abolfathi et al. 2017, DR14) containing 2812 datacubes. The galaxy masses range from $\sim 10^9 - 10^{11}\ M_\odot$. The Primary and Color-enhanced samples of MaNGA, together known as the Primary+ sample, contains 1700 galaxies, out of which 970 are early-type. These were selected using Galaxy Zoo (Lintott et al. 2011; Willett et al. 2013) morphologies and visually inspected when necessary (Goddard et al. 2017).

**Table 1.** Median velocity dispersion, effective radius and redshift of the mass terciles.

| Mass range ($\log M/M_\odot$) | $\sigma$ (km/s) | $R_e$ (kpc) | z |
|---|---|---|---|
| 9.9 – 10.2 | 130 | 2.43 | 0.027 |
| 10.2 – 10.5 | 170 | 3.11 | 0.030 |
| 10.5 – 10.8 | 200 | 4.38 | 0.034 |

# Распределение по массам

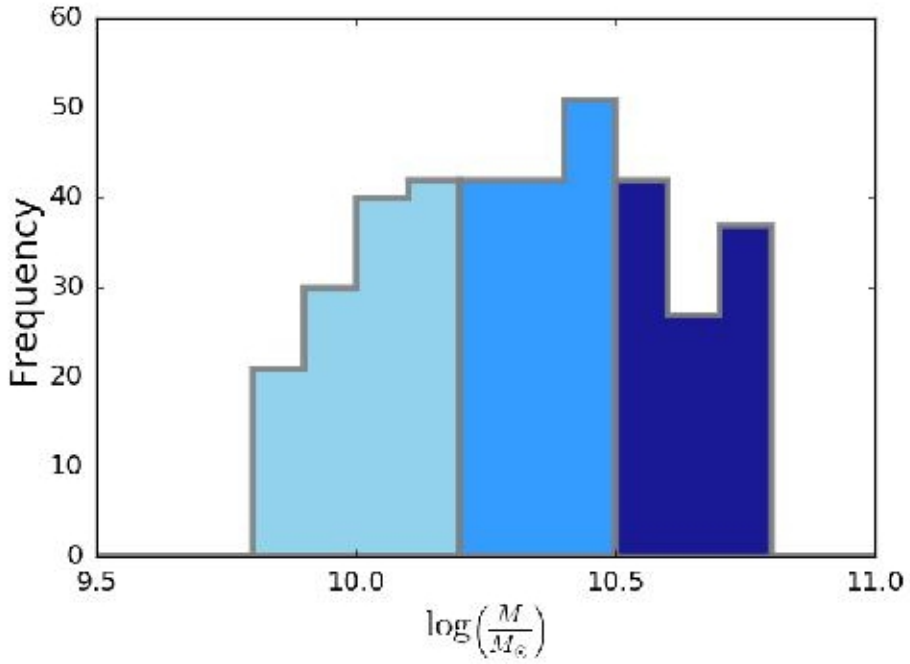


**Figure 3.** Masses of our sample of 366 early type galaxies, split into 3 bins containing equal numbers of galaxies.

# Посчитали по суммарным спектрам индексы

**Table 2.** Index definitions for the absorption features used in this work. All wavelengths are in vacuum. The optical indices are defined in Trager et al. (1998); NaI in (La Barbera et al. 2013); and FeH in Conroy & van Dokkum (2012a).

| Index | Blue Continuum | Feature | Red continuum |
|---|---|---|---|
| H$\beta$ | 4829.2 - 4849.2 | 4849.2 - 4878.0 | 4878.0 - 4893.0 |
| Mg$b$ | 5144.1 - 5162.8 | 5161.6 - 5194.1 | 5192.8 - 5207.8 |
| Fe5270 | 5234.6 - 5249.6 | 5247.1 - 5287.1 | 5287.1 - 5319.6 |
| Fe5335 | 5306.1 - 5317.4 | 5313.6 - 5353.6 | 5354.9 - 5364.9 |
| NaD | 5862.2 - 5877.3 | 5878.5 - 5911.0 | 5923.8 - 5949.8 |
| NaI | 8145.2 - 8155.2 | 8182.2 - 8202.3 | 8235.3 - 8246.3 |
| FeH | 9855.0 - 9880.0 | 9905.0 - 9935.0 | 9940.0 - 9970.0 |

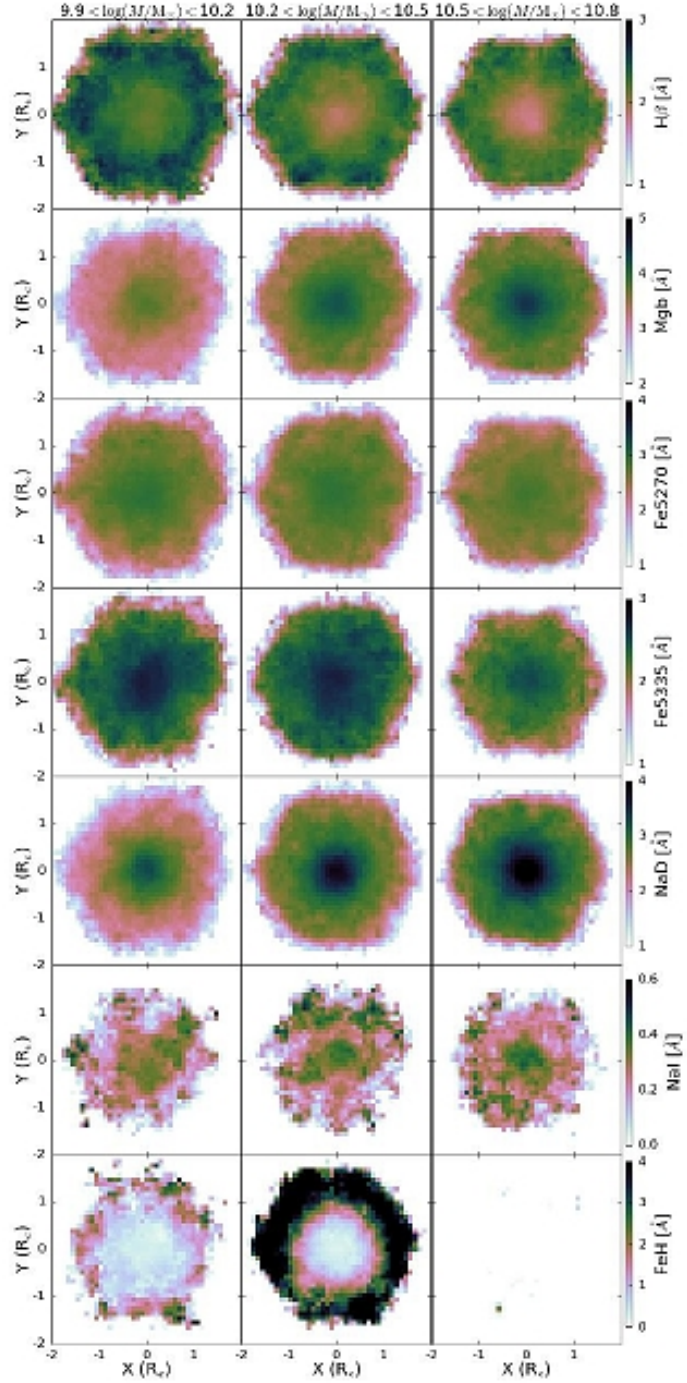
9.9 < log(M/M⊙) < 10.2
10.2 < log(M/M⊙) < 10.5
10.5 < log(M/M⊙) < 10.8
Y (Re)
X (Re)
Hβ (Å)
Mgb (Å)
Fe5270 (Å)
Fe5335 (Å)
NaD (Å)
NaI (Å)
FeH (Å)

# Параметры звездного населения по радиусу

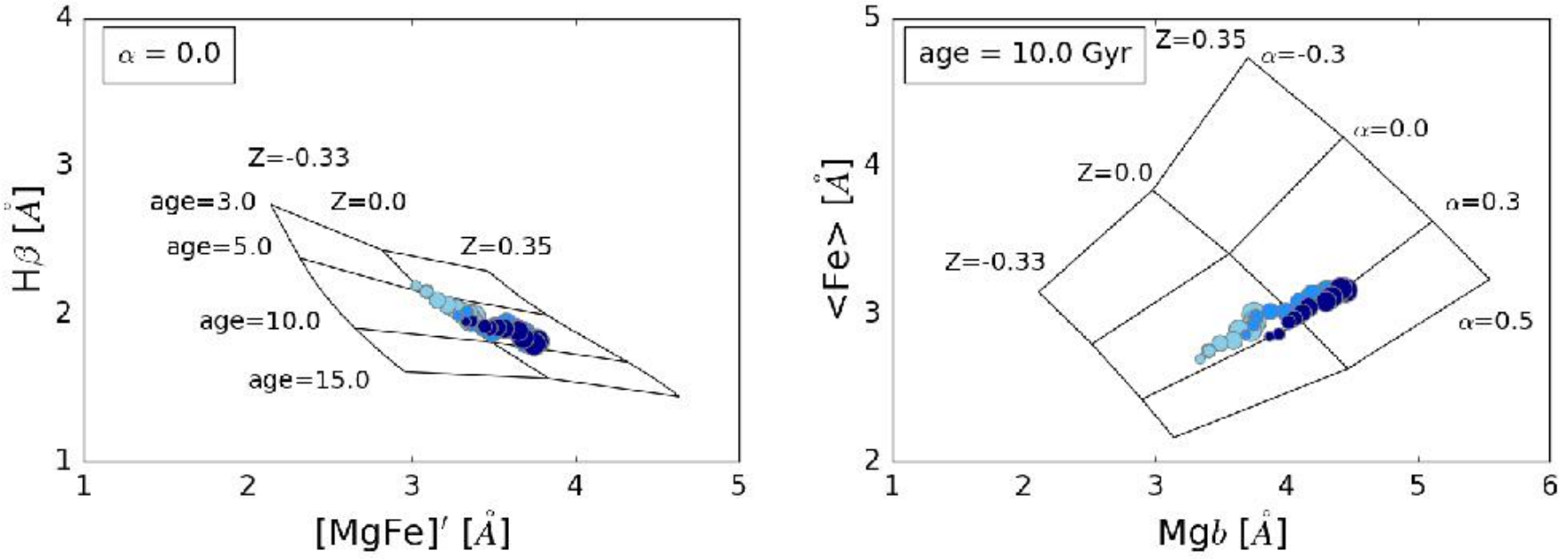


**Figure 10.** Optical indices for the three mass bins against the high-resolution TMJ model index grids. The age and metallicity dependence plotted for models with $[\alpha/\mathrm{Fe}] = 0$ (left-hand panel) and metallicity against $[\alpha/\mathrm{Fe}]$ for models at a fixed age of 10 Gyr (right-hand panel). Dark to light shades of blue represent the mass bins in decreasing order; decreasing size represents increasing radius.

# Наклон НФМ по инфракрасной линии натрия

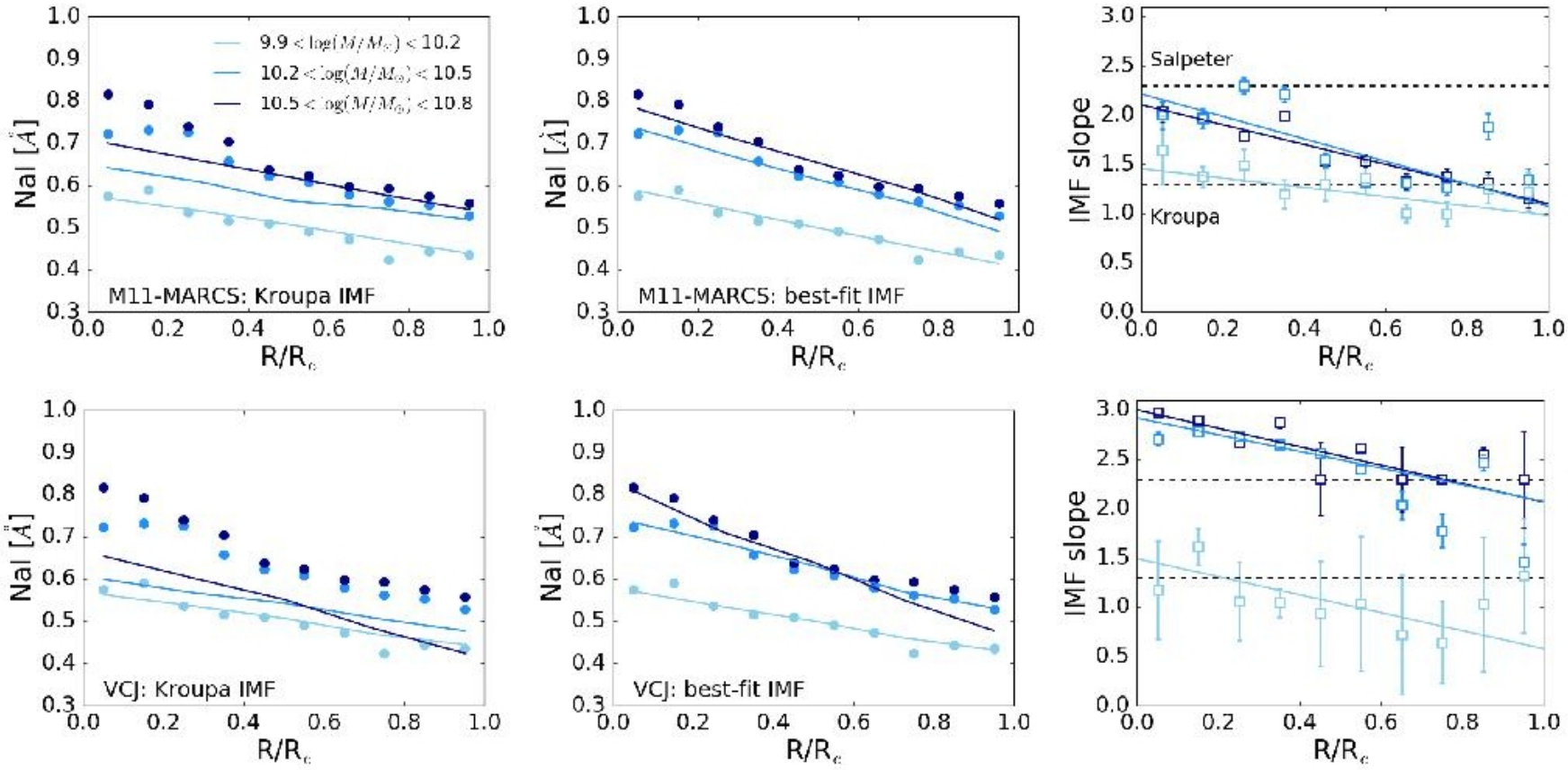


**Figure 14.** NaI line-strengths for the mass bins as a function of radius, with 1-$\sigma$ errors calculated using a Monte Carlo-based analysis, and stellar population model fittings using M11-MARCS (top panels) and VCJ (bottom panels). *Left-hand panels*: Models shown as lines for a Kroupa IMF with the age, metallicity, [$\alpha$/Fe] and [Na/Fe] as derived in Sections 3.1 and 3.2. *Middle panels*: Models (lines) with varying IMF. *Right-hand panels*: Open squares show the IMF slopes of the best-fit models shown in the middle panels.

# То же самое по полосе Wing-Ford

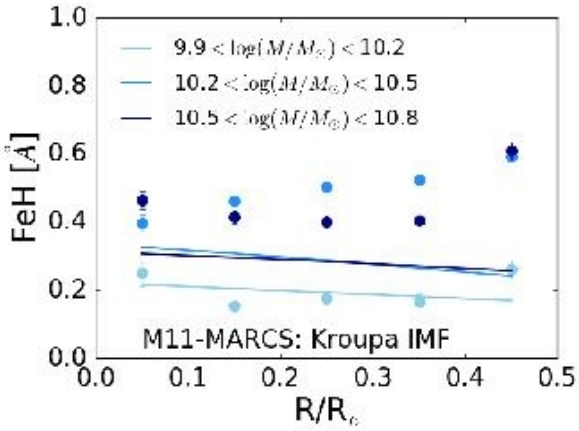


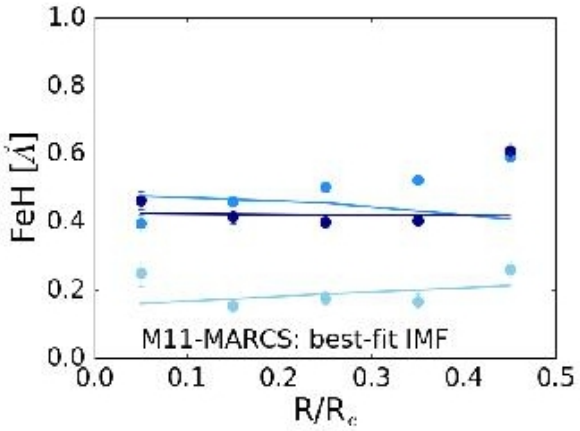


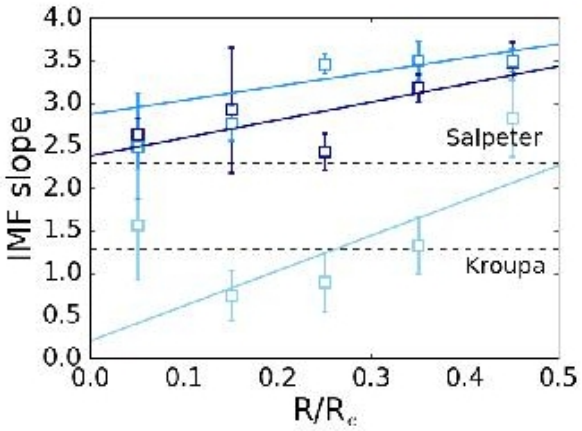


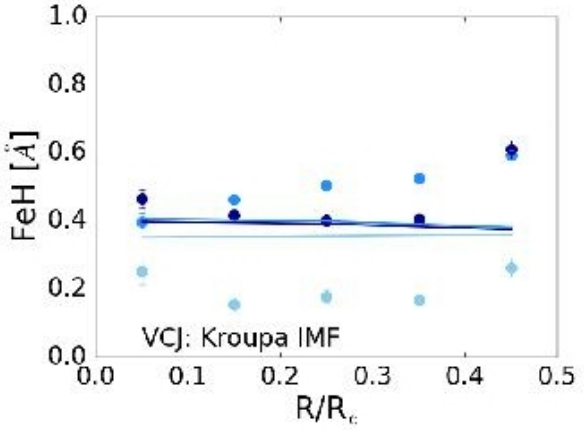


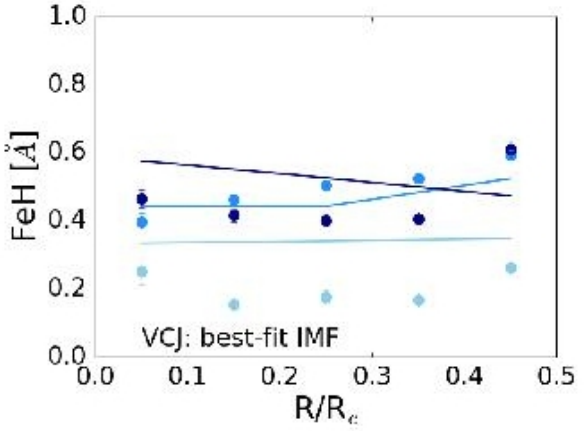


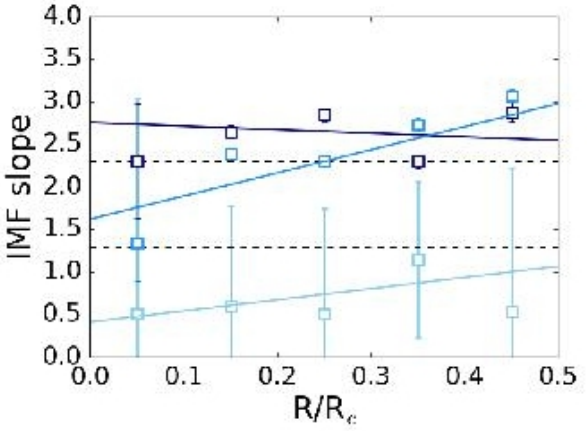

# Выводы

- Как индикатор наклона НФМ, выбрали естественно линию натрия;
- А про FeH полосу сказали, что там небо плохо вычитается.
- И тогда наклон IMF падает вдоль радиуса, что они связывают с локальной дисперсией скоростей звезд.

# Astro-ph: 1803.07082

## A new strong-lensing galaxy at z=0.066: Another elliptical galaxy with a lightweight IMF

William P. Collier,* Russell J. Smith, John R. Lucey
*Centre for Extragalactic Astronomy, Departments of Physics, University of Durham, Durham DH1 3LE, UK*

Submiteed to MNRAS 16th March 2018

**ABSTRACT**

We report the discovery of a new low-redshift galaxy-scale gravitational lens, identified from a systematic search of publicly available MUSE observations. The lens galaxy, 2MASXJ04035024-0239275, is a giant elliptical at $z = 0.06604$ with a velocity dispersion of $\sigma = 314\,\mathrm{km\,s^{-1}}$. The lensed source has a redshift of 0.19165 and forms a pair of bright images either side of the lens centre. The Einstein radius is 1.5 arcsec, projecting to 1.8 kpc, which is just one quarter of the galaxy effective radius. After correcting for an estimated 19 per cent dark matter contribution, we find that the stellar mass-to-light ratio from lensing is consistent with that expected for a Milky Way initial mass function (IMF). Combining the new system with three previously-

# Поиски эмиссионных объектов в полях MUSE

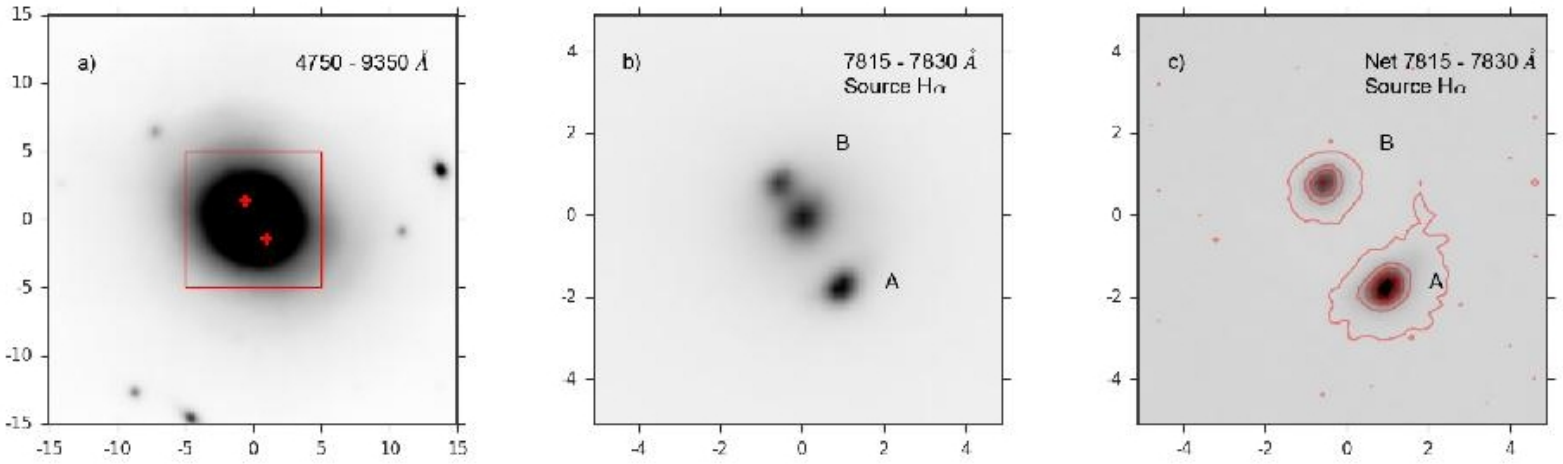


**Figure 1.** MUSE data of J0403, within different wavelength ranges (shown in the top right). a) displays a broadband image collapsed over the entire MUSE wavelength range, displaying the lens structure. The red crosses mark the arc positions, while the red box encompasses the region shown in panels b) and c). In b) we collapse about the H$\alpha$ line in the background source, revealing arcs A and B, separated by $2.94 \pm 0.06$ arcsec, without the need for lens subtraction. c) shows the continuum-subtracted image at the same wavelength, with contours to show the outer isophotes of the arcs.

# Случайно нашли гравлинзу

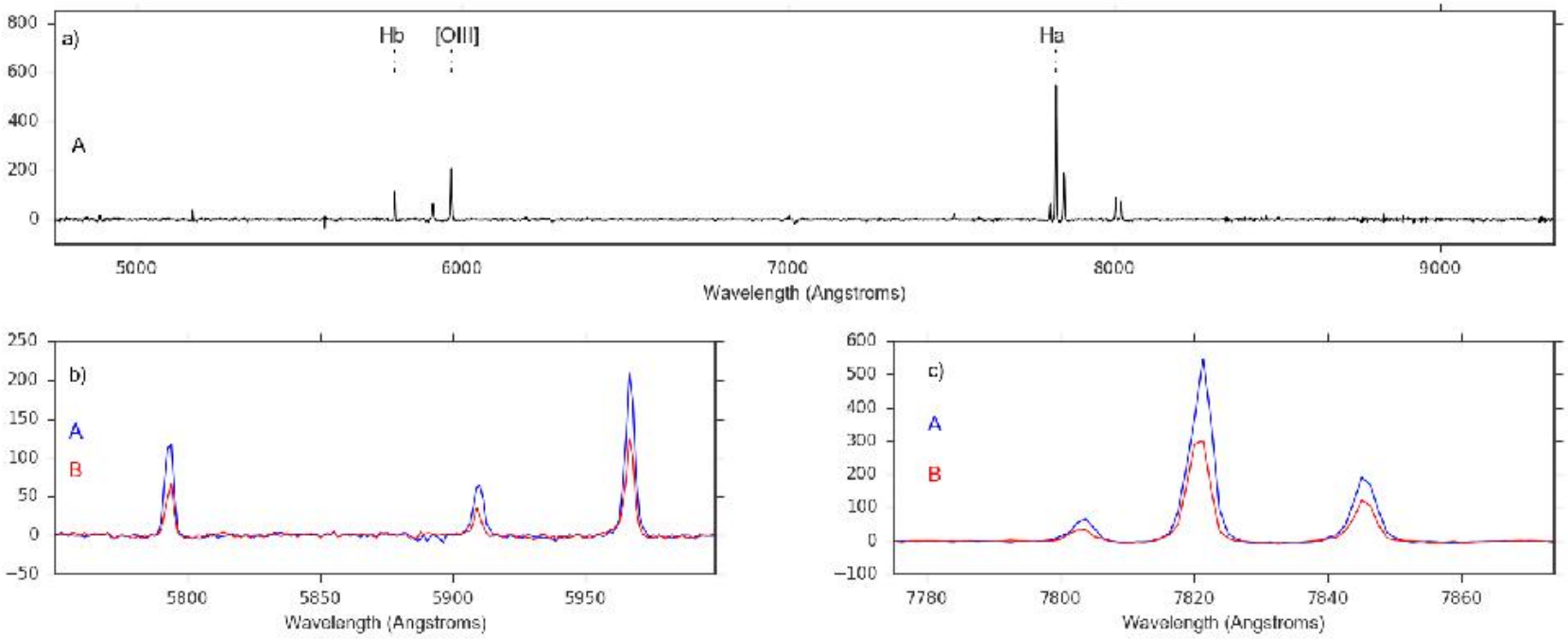


**Figure 2.** MUSE spectra of the lensed images. In a) we display the arc spectrum extracted from a continuum-subtracted residual datacube, showing the bright H$\alpha$, [N II], [O III], H$\beta$, H$\gamma$ and [S II] emission lines, at a redshift of 0.19165. In b) and c), we overlay the emission from images A and B, for the [OIII] and H$\alpha$ regions, respectively. There is negligible velocity offset ($\lesssim 50$ km s$^{-1}$) between the two spectra, and image A has been subject to a greater magnification.

# Если это гравлинза, она решается:

($z_{\rm CMB} = 0.06569, 0.19130$ and $\frac{D_{\rm l} D_{\rm s}}{D_{\rm ls}} = 400.5\,{\rm Mpc}$). We derive a total projected mass, $M_{\rm Ein} = 10.64 \pm 0.23 \times 10^{10}\ {\rm M}_{\odot}$, with the 2 per cent uncertainty dominated by the measurement of $R_{\rm Ein}$. Including a small ellipticity ($e \approx 0.1$ as measured from GALFIT) increases the mass by 3 per cent, and the inclusion of a small external shear (< 5/1 per cent for SIS/SIE) reproduces the image positions perfectly. In order to account for these additional possible complexities, we revise the uncertainty in $M_{\rm Ein}$ to ~4 per cent, i.e. $0.4 \times 10^{10}\,{\rm M}_{\odot}$.

The DM mass component is estimated following Smith et al. (2015), using the EAGLE hydrodynamical cosmological simulation (Schaye et al. 2015). We measure the average DM mass which would be projected inside an aperture of 1.8 kpc, averaged over all EAGLE halos hosting galaxies with stellar velocity dispersions $>275\,{\rm km\,s^{-1}}$. This indicates a contribution of $\mathrm{M}_{\rm Ein}^{\rm DM} = 2.01 \pm 0.36 \times 10^{10}\,{\rm M}_{\odot}$ (i.e. 19% of $\mathrm{M}_{\rm Ein}$), which yields an aperture stellar mass $M_{\rm Ein}^{*}$ of $8.63 \pm 0.54 \times 10^{10}\,{\rm M}_{\odot}$.

# … и вычисляется отношение полной массы к светимости!

The final corrected Einstein-aperture apparent magnitude is $i_{\rm Ein} = 15.87 \pm 0.05$, which for the adopted cosmology ($D_{\rm L} = 295.7$ Mpc), and the solar AB $i$–band absolute magnitude of 4.534 (Blanton & Roweis 2007), yields an aperture luminosity of $2.59 \pm 0.12 \times 10^{10}\,{\rm L}_{\odot}$. The uncertainty is dominated by the applied corrections. Combined with $M^{*}_{\rm Ein}$ the observed stellar mass-to-light ratio is $\Upsilon = 3.33 \pm 0.26$ solar units.

After making this correction to remove the emission-infilling of the spectrum at H$\beta$, we perform a full-spectrum fit over the interval 4500–6400 Å, using single-burst models from Conroy & van Dokkum (2012b), (Figure 3, green). We allow for variation in abundances of Mg, Fe, Na, and C, as well as variation in age. Formally, the fit implies an old population, with age $12.0 \pm 1.0$ Gyr, high metallicity $[{\rm Z/H}] \approx [{\rm Mg/H}] \approx +0.15 \pm 0.02$ and typical massive elliptical galaxy abundance ratios $[{\rm Mg/Fe}] \approx +0.3$, $[{\rm Na/Fe}] \approx +0.5$, $[{\rm C/Fe}] \approx +0.2$.

The reference mass-to-light ratio is estimated with Conroy et al. (2009) stellar population models accessed via EZGAL (Mancone & Gonzalez 2012). For a Kroupa (2001) IMF, with an old, solar metallicity stellar population ($z_{\rm form} = 3$), the models predict $\Upsilon^{*}_{\rm Ref} = 2.90 \pm 0.10$. The uncertainty is derived from small variations in the metallicity and age (e.g. $z_{\rm form} = 2.5$–$3.5$, metallicity 1–1.5 solar). The resulting IMF mass excess parameter, with its statistical error is $\alpha = 1.15 \pm 0.10$.

# … которое сравнивается с тем, что должно иметь звездное население с измеренными параметрами

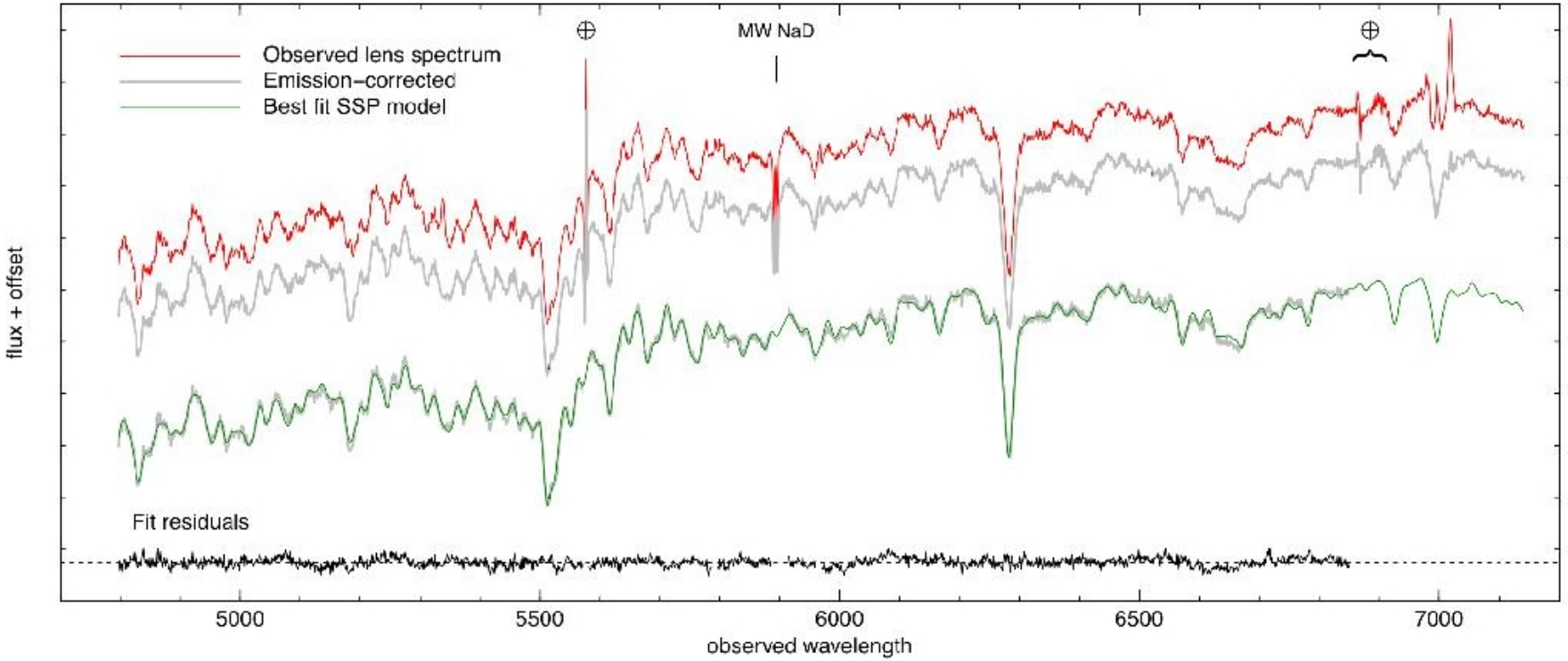


**Figure 3.** The MUSE spectrum of the lens galaxy J0403, extracted within the Einstein aperture, i.e. radius 1.5 arcsec, after masking pixels strongly affected by the arcs. For clarity, only the blue region used for fitting stellar population models is shown. The observed spectrum (red) shows that the galaxy has an absorption-dominated spectrum, but also has a nebular line emission component, seen most easily in the H$\alpha$–[N II] region. The corrected spectrum, shown in grey, after subtracting an emission-line model, fitted to the H$\alpha$–[N II] complex, and assuming Case B recombination and galactic (no internal) extinction, to predict the H$\beta$ emission. Below, we reproduce the emission-corrected spectrum, and show the best-fitting stellar population (green), derived from the models of Conroy & van Dokkum (2012a). This model has age 12 Gyr and metal abundances typical for massive ellipticals. The fit residuals, shown in black, have a 1 per cent rms. In fitting this model, we exclude the H$\alpha$ region, as well as wavelengths contaminated by atmospheric artifacts (indicated by

# И получается, то оно, как и 3 предыдущих гравлинзы, согласуется с НФМ Крупа

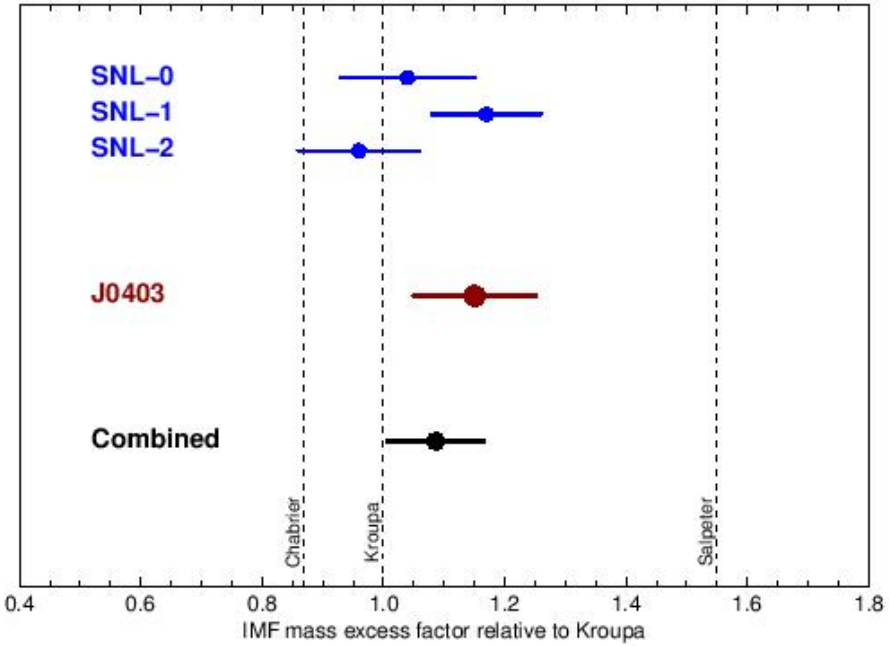


**Figure 4.** The distribution of the mass excess parameter ($\alpha$) for the combined SNELLS and J0403 sample. In blue, is the SNELLS sample with results for SNL-0 from Newman et al. (2017), and SNL-1, SNL-2 from Collier et al. (2018). The result for J0403 from this paper is marked in red. The sample average is $\langle\alpha\rangle = 1.09 \pm 0.08$, with an inferred *intrinsic* scatter of $< 0.32$, at 90 per cent confidence. These galaxies on average favour a Milky-Way like IMF in preference to a Salpeter or heavier IMF.